TRANSPORT PROBLEMS 2023 Volume 18 Issue 3
PROBLEMY TRANSPORTU DOI:10.20858/tp.2023.18.3.02

Keywords: crashworthiness; railway safety; passive safety; energy absorption

Aleksandra LISOWSKA[1]*, Henryk SANECKI[2], Maciej SZKODA[3]

SIMULATION METHOD FOR MEASURING THE IMPACT ENERGY OF RAIL VEHICLES EQUIPPED WITH A SOFT ABSORBER

Summary. This paper presents a simulation method for testing the energy absorbed by the absorption systems of rail vehicles equipped with a soft absorber. The method makes it possible to verify the actual behavior of the absorption system during the impact of two vehicles. The first part of this paper describes the structural elements of a railway vehicle performing the function of an energy absorber during an impact according to the EN 15227 standard. A soft absorber, the so-called honeycomb, is analyzed in detail. It is a multicellular structure often used in rail vehicles due to its properties of controlled deformation. The literature review describes the research conducted on this element. The analytical part of this paper describes a general mathematical model of a rail vehicle collision according to Scenario 1, in which the collided vehicles are of the same type, and Scenario 2 for vehicles of different types. A computational impact simulation for the two scenarios has been carried out using the specialist software Mathcad, and the results are presented in graphs. The paper ends with conclusions presenting the application possibilities of the developed tool.

1. INTRODUCTION

As the economic level of each country increases, so does the need for rail transport. This branch of transport plays a crucial role in the economy, allowing goods and people to be moved around. The popularity of railways is due to many factors, one of which is the high level of safety. Safety in rail transport depends on many factors. These mainly include the organization of transport and traffic, the technical condition of rolling stock and infrastructure, and the professional qualifications of staff and the way in which they carry out their duties. However, rail is a relatively safe form of transport, and the statistics seem to confirm this. In 2020, there were a total of 1331 significant accidents in the European Union, with 687 fatalities. The vast majority of adverse events resulted from pedestrians or motor vehicles encroaching on the track [1]. Collisions between two railway vehicles usually represent a small proportion of adverse events (e.g., in 2020, there were a total of 13 collisions, representing less than 2% of all incidents within European Union countries).

Nevertheless, as demand for rolling stock increases, so does the likelihood of collisions. It is therefore worth considering the question of the structural safety of modern vehicles. During a collision between two railway units, the engine drivers are the most vulnerable to death or serious injury because it is the extreme parts of the train that are damaged during an accident [2]. It is for this reason that various design solutions have started to be implemented to protect engine drivers. According to EN 15227, passive

[1] Cracow University of Technology, Department of Rail Vehicles and Transport; al. Jana Pawla II 37, 31-864 Krakow, Poland; e-mail: aleksandra.lisowska@pk.edu.pl; orcid.org/0000-0001-8767-4806
[2] Cracow University of Technology, Department of Rail Vehicles and Transport; al. Jana Pawla II 37, 31-864 Krakow, Poland; e-mail: henryk.sanecki@pk.edu.pl; orcid.org/0000-0002-6319-9112
[3] Cracow University of Technology, Department of Rail Vehicles and Transport; al. Jana Pawla II 37, 31-864 Krakow, Poland; e-mail: maciej.szkoda@pk.edu.pl; orcid.org/0000-0002-9511-2253
* Corresponding author. E-mail: aleksandra.lisowska@pk.edu.pl

safety elements are to provide protection against climbing phenomena (anti-climbing systems), offer a safe survival zone for the driver, reduce deceleration, and above all, absorb energy during an impact by dissipating kinetic energy [3]. The latter role is fulfilled by suitable structural components manufactured from highly ductile materials. These components include railway buffers, a controlled crumple zone, and absorbers, including soft absorbers (so-called honeycombs) [4].

2. THE SOFT ABSORBER AS A PART OF IMPACT ENERGY ABSORPTION

A soft absorber, or a so-called honeycomb, is an object with thin walls and a multicellular structure. It is used in the railway industry quite often due to its strength-to-weight ratio, especially in the case of high-speed railways, where the absorber system has to absorb a very large amount of energy during an impact [5-7]. Honeycombs used in railways are made of aluminum, mainly due to its low stiffness and density, controlled deformation, and stable impact force [8]. Composite materials are also used due to their lightness and environmental benefits [9]. It is also worth emphasizing the low cost of using this solution [10, 11]. Researchers from all over the world have studied the ability of thin-walled honeycomb structures to absorb energy during an impact, and the pioneer in this field was J.M. Alexander [12], who studied the problem of the collapse of axially compressed cylindrical pipes. The static and dynamic properties of thin-walled circular, square, and multicellular structures were studied. Calculations, simulations, and experiments on real objects were carried out.

In order to verify the actual amount of energy absorbed by a component or set of components, a crash test should be carried out [13]. Its purpose is to confirm the computer simulation and crashworthiness calculations based on the requirements in EN 15227. There is also a need for tests to calibrate theoretical models. Nowadays, most such tests are performed using the finite element method, and for the simulation of crash tests of railway vehicles, the LS Dyna software is most commonly applied [14]. This method is highly accurate and offers a wide range of possibilities, but it is time-consuming and expensive. Therefore, in order to optimize the time and costs needed for the simulation of the impact with the use of the finite element method, it is worth using a mathematical model that enables an initial verification of the behavior of the absorption system. This is what the method presented in this paper offers.

3. SIMULATION OF CRASH TESTS

In this paper, collision scenarios are analyzed according to which railway vehicles may hit vehicles of the same type (Scenario 1 according to PN-EN 15227) or another type (Scenario 2 according to PN-EN 15227). Fig. 1 presents schemes of such cases numerically simulated in the paper. Fig. 1a shows a collision of two identical vehicles on the route according to Scenario 1. Fig. 1b shows an experimental collision according to Scenario 1, where the second vehicle is replaced by a test car with a so-called rigid headwall. Instead of a whole train set, a model containing one lead car with an appropriately chosen equivalent mass and speed is considered. The effects of buffers and couplings connecting the wagons are neglected. All dynamic effects related to the behavior of the bogies are also neglected.

3.1. General mathematical model of vehicle collision

The general formula for the kinetic energy of a vehicle immediately before impact, which forms the basis for further considerations in this paper, is as follows:

$$E_{\mathrm{k}} = \frac{1}{2} \cdot m \cdot v^2, \tag{1}$$

where

$$m = m_{\mathrm{p}} + 2 \cdot m_{\mathrm{w}} + \frac{1}{2} \cdot m_{\mathrm{o}} \tag{2}$$

v - vehicle speed,
m - calculated mass of the vehicle,
m_p - weight of the wagon body,
m_w - mass of one bogie, and
m_o - total mass of passengers.

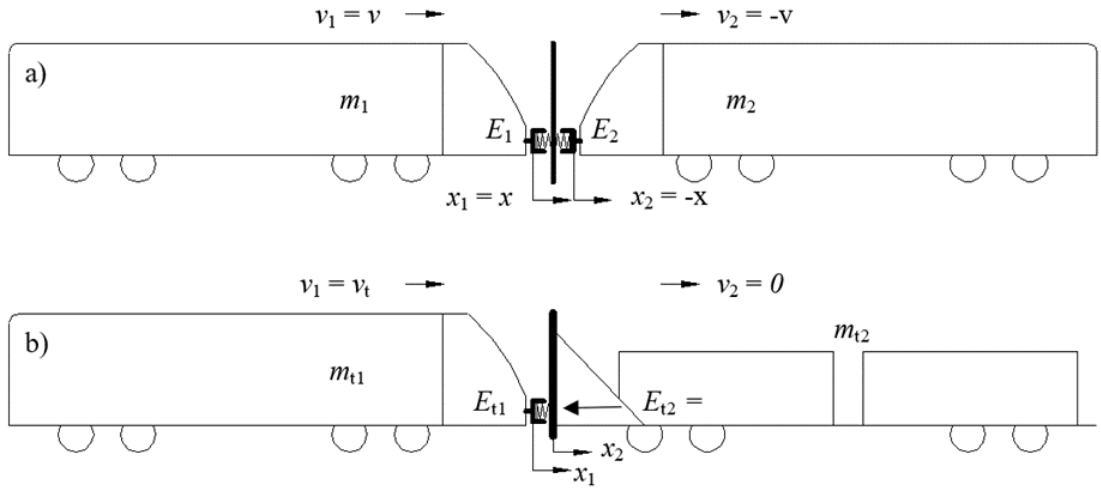

Fig. 1. Schematics of simulated crashes: a) a crash between two identical vehicles on the route according to Scenario 1 and b) an experimental crash according to Scenario 1 (the second vehicle is replaced by a test wagon)

The collision itself can be described as follows. Suppose that two bodies with masses m_1 and m_2 and initial velocities v_1 and v_2 collide perfectly inelastically. Let both velocities have the same direction and let v_1 be greater than v_2 (that is, the first body catches up with the second). During the collision, the two bodies are deformed and joined so that after the collision, they move together with velocity u. During this collision, there are no conservation forces acting in the isolated system, and therefore, no mechanical energy is conserved. On the other hand, momentum is conserved, from which the following formula is derived:

$$m_1 v_1 + m_2 v_2 = (m_1 + m_2)u. \tag{3}$$

Hence, the common velocity after the collision is

$$u = \frac{m_1 v_1 + m_2 v_2}{m_1 + m_2}. \tag{4}$$

Knowing the kinetic energy of both bodies before the collision, as well as the kinetic energy of the solid formed as a result of the collision, one can calculate the loss of kinetic energy converted into other forms of energy:

$$E = \frac{1}{2} m_1 v_1^2 + \frac{1}{2} m_2 v_2^2 - \frac{1}{2}(m_1 + m_2)u^2. \tag{5}$$

Ultimately,

$$E = \frac{1}{2} \frac{m_1 m_2}{m_1 + m_2}(v_1 - v_2)^2 = \frac{1}{2} m_e {v_0}^2. \tag{6}$$

The product of the two colliding masses divided by their sum represents the so-called reduced mass m_e of the system. The difference between velocities $v_1 - v_2$ is the relative velocity v_0. Thus, the loss of kinetic energy transformed during an inelastic collision into other types of energy is proportional to the reduced mass of the system and the square of the relative velocity.

3.1.1. Collision of two identical vehicles on the route

First, a simulation of a real-world collision between two identical vehicles was considered, as shown in the diagram in Fig. 1a. According to EN 15227, this is Scenario 1.

We assume perfect symmetry of the vehicles and that their behavior during the collision is the same. Therefore, we can write

$$m_1 = m_2 = m, \tag{7}$$

$$x_2 = -x_1 = -x, \tag{8}$$

and

$$v_1 = v,\ v_2 = -v. \tag{9}$$

Following the examples analyzed in the monograph [15], we describe the problem using the conservation of momentum principle:

$$m_1 v_1 + m_2 v_2 = m_1 \dot{x}_1 + m_2 \dot{x}_2. \tag{10}$$

However, the result is only an identity: $0 \equiv 0$. In contrast, applying the principle of conservation of energy gives the following result:

$$\frac{1}{2} m_1 v_1^2 + \frac{1}{2} m_2 v_2^2 = \frac{1}{2} m_1 \dot{x}_1^2 + \frac{1}{2} m_2 \dot{x}_2^2 + E \tag{11}$$

or

$$m v^2 = m \dot{x}^2 + E. \tag{12}$$

After simple transformations, we obtain

$$\dot{x}^2 = v^2 - \frac{E}{m}, \tag{13}$$

and after substituting the formula, we get

$$E = E_1 + E_2 = 2E_1. \tag{14}$$

Then, after two-sided differentiation, we finally obtain a differential equation of the form

$$\dot{x}\ddot{x} = -\frac{1}{m}\frac{dE_1}{dt}. \tag{15}$$

3.1.2. Mathematical models for experimental tests

The experimental tests are mainly aimed at calibrating the theoretical model. Experimental tests are performed only according to Scenarios 1 or 2.

Instead of actual masses, the test vehicles have masses m_{t1} and m_{t2}. One of the vehicles (m_{t2}) is the block (i.e., a stationary, unbraked special test wagon) (Fig 1(b)). For Scenario 1, the block is a test wagon with a rigid blocking plate. In the test for Scenario 2, a freight wagon containing ballast in the form of loose material is used. The mass m_{t2} may vary in time (e.g., due to the sloshing of the loose ballast against the walls of the wagon).

The above assumptions can be written as follows:

$$x = x_1 - x_2 \tag{16}$$

$$m_{t1} = \text{const}(t),\ m_{t2}(t),\ \mu_t(t) = \frac{m_{t1}}{m_{t2}(t)} \tag{17}$$

$$v_1 = v_t,\ v_2 = 0. \tag{18}$$

According to [15], we have two equations:

$$\begin{cases} m_{t1}v_t + m_{t2}0 = m_{t1}\dot{x}_1 + m_{t2}\dot{x}_2 \\ \frac{1}{2}m_{t1}v_t^2 = \frac{1}{2}m_{t1}\dot{x}_1^2 + \frac{1}{2}m_{t2}\dot{x}_2^2 + E_{t1} + E_{t2} \end{cases} \tag{19}$$

By the appropriate transformations of the above equations, the final form of the differential equation can be obtained:

$$\ddot{x}\,\dot{x} = -\frac{1}{2}\dot{\mu}_t \frac{v_t^2 - \dot{x}^2}{1+\mu_t} - (1+\mu_t)\cdot\frac{\dot{E}_{t1}+\dot{E}_{t2}}{m_{t1}}. \tag{20}$$

If the mass of the test vehicle constituting the block is constant (i.e., when $m_{t2} = \text{const}(t)$), then $\mu_t = \text{const}(t)$ and Equation (20) will take the form of

$$\ddot{x}\,\dot{x} = -(1+\mu_t)\cdot\frac{\dot{E}_{t1}+\dot{E}_{t2}}{m_{t1}}. \tag{21}$$

3.2. Simulation of impact tests including absorbers

The analyzed energy-absorbing system consists of two buffers as well as an absorber proper (i.e., a so-called honeycomb) (Fig. 2). The absorber starts to deform under the influence of a relatively small compressive force P_a, which is below the maximum force transmitted by the buffers P_z [16]. In order to absorb the required amount of energy, the absorber must have a sufficient stroke l_a, which can be pre-calculated. The formula for its length is determined below.

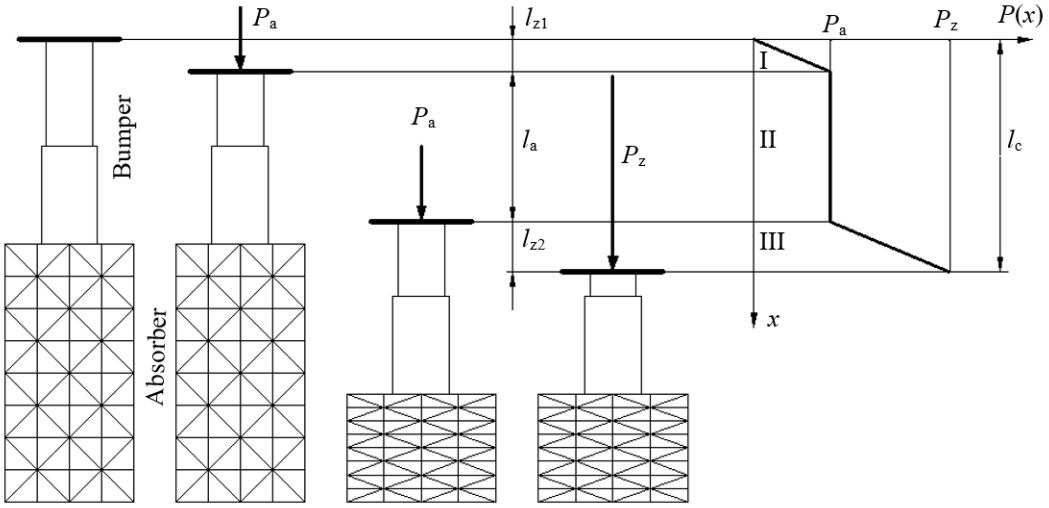

Fig. 2. Diagram of the absorption system comprising a buffer (range I and III) and a honeycomb absorber (range II), the consecutive stages of the system and its characteristics, and forces and displacements

The following designations were used for the passenger vehicle absorption system:

P_a – load force on the absorber,
P_z – maximum force on buffers,
v – vehicle speed,
k – stiffness of the pair of buffers,
x, x_1, x_2 – coordinates defining the position of the vehicles,
m, m_1, m_2 – masses of the colliding vehicles,
v, v_1, v_2 – speeds of the colliding vehicles,
l_{z1}, l_{z2} – buffer working lengths,
l_a – absorber stroke length,
λ – auxiliary size (ratio of buffer lengths), and
E_1, E_2, E_{ua} – energy absorbed by the absorption device of one vehicle.

According to Fig. 2, the energy that can be absorbed by the buffers is

$$E_{\mathrm{zd}} = \frac{1}{2} \cdot k \cdot l_z^2, \tag{22}$$

where

$$l_z = l_{z1} + l_{z2}. \tag{23}$$

Hence, the formula for bumper stiffness is

$$k = \frac{2 \cdot E_{\mathrm{zd}}}{l_z^2}. \tag{24}$$

Using the following formulae for the forces in the bumpers, we obtain

$$P_{\mathrm{z}} = k \cdot l_z\ ,\ P_{\mathrm{a}} = k \cdot l_{z1}\ \text{ oraz } P_{\mathrm{a}} = \lambda \cdot P_z, \tag{25}$$

where

$$\lambda \cong 0{,}6 \div 1. \tag{26}$$

The formula for the energy absorbed by the absorbing system (as shown in Fig. 2) can be obtained with the following formula:

$$E_{\mathrm{ua}} = P_{\mathrm{a}} \cdot [\tfrac{1}{2} \cdot l_{z1} + (l_a + l_{z2}) + \tfrac{1}{2} \cdot \tfrac{l_{z2}^2}{l_{z1}}] \tag{27}$$

or

$$E_{\mathrm{ua}} = P_{\mathrm{a}} \cdot [l_a + \tfrac{(l_{z1}+l_{z2})^2}{2l_{z1}}]. \tag{28}$$

The final energy absorbed by the absorption system is calculated as

$$E_{\mathrm{ua}} = P_{\mathrm{a}} \cdot \left[l_a + \tfrac{l_z^2}{2l_{z1}}\right]. \tag{29}$$

Since $E_{\mathrm{ua}} = E_{\mathrm{k}}$, it is possible to determine the size (length) of the absorber stroke needed to transfer kinetic energy as

$$l_{\mathrm{a}} = \frac{E_{\mathrm{k}}}{P_a} - \frac{l_z^2}{2l_{z1}} = \frac{m \cdot v^2}{2 \cdot \mathrm{P_a}} - \frac{l_z^2}{2l_{z1}}. \tag{30}$$

Meanwhile, overall length is calculated as

$$l_{\mathrm{c}} = l_z + l_a. \tag{31}$$

Considering the diagram in Fig. 2, we have the following function for the energy absorbed by one absorbing system at a given instant *t:*

$$E_1 = \begin{cases} \frac{1}{2}kx^2 & for\ range\ I \\ \frac{1}{2}kl_{z1}^2 + P_{\mathrm{a}}(x - l_{z1}) & for\ range\ II \\ \frac{1}{2}kl_{z1}^2 + P_{\mathrm{a}}(x - l_{z1}) + \frac{1}{2}k(x - l_{z1} - l_{\mathrm{a}})^2 & for\ range\ III \end{cases}. \tag{32}$$

Alternatively, with the division into three ranges, we get

$$E = 2E_1 = P_{\mathrm{a}} \begin{cases} \frac{x^2}{l_{z1}} \\ 2x - l_{z1} \\ 2x - l_{z1} + \frac{(x - l_{z1} - l_{\mathrm{a}})^2}{l_{z1}} \end{cases}. \tag{33}$$

3.2.1. Impact in Scenario 1 with a soft absorber system

The solution for Scenario 1 is shown below (Fig. 1a). Two identical vehicles collide head-on with an equal speed *v*. Each vehicle has a single-stage energy absorbing system, which is described by Equation (33). When Equation (33) is substituted into the energy balance Equation (15), the following equation is obtained:

$$\dot{x}^2 = v^2 - \frac{E}{m} = v^2 - \frac{P_\mathrm{a}}{m}\begin{cases} \frac{x^2}{l_{z1}} \\ 2x - l_{z1} \\ 2x - l_{z1} + \frac{(x - l_{z1} - l_\mathrm{a})^2}{l_{z1}} \end{cases}, \tag{34}$$

where

$$x = x_1 = -x_2. \tag{35}$$

When Equation (34) is differentiated on both sides, it takes the form of

$$2\dot{x}\ddot{x} = -\frac{P_\mathrm{a}}{m}\begin{cases} \frac{2x\dot{x}}{l_{z1}} \\ 2\dot{x} \\ 2\dot{x} + \frac{2(x - l_{z1} - l_\mathrm{a})}{l_{z1}}\dot{x} \end{cases}, \tag{36}$$

and after transformations, it takes the following form:

$$\ddot{x} + \frac{P_\mathrm{a}}{m l_{z1}}\begin{cases} x \\ l_{z1} \\ x - l_\mathrm{a} \end{cases} = 0. \tag{37}$$

If we divide Equation (37) by l_c and substitute

$$\xi = \frac{x}{l_c},\ w = \frac{P_\mathrm{a}}{m l_{z1}},\ \lambda_{z1} = \frac{l_{z1}}{l_\mathrm{c}},\ \lambda_{z2} = \frac{l_{z2}}{l_\mathrm{c}},\ \lambda_\mathrm{a} = \frac{l_\mathrm{a}}{l_\mathrm{c}},\ \lambda_\mathrm{c} = \frac{l_{z1} + l_\mathrm{a} + l_{z2}}{l_c} = 1, \tag{38}$$

we obtain

$$\ddot{\xi} + w \cdot g(\xi) = 0, \tag{39}$$

where the dimensionless function $g(\xi)$ is described by the formula:

$$g(\xi) = \begin{cases} \xi & \text{dla } 0 \le \xi \le \lambda_{z1} \\ \lambda_{z1} & \text{dla } \lambda_{z1} < \xi \le \lambda_{z1} + \lambda_\mathrm{a} \\ \xi - \lambda_\mathrm{a} & \text{dla } \lambda_{z1} + \lambda_\mathrm{a} < \xi \le \lambda_\mathrm{c} \end{cases}. \tag{40}$$

We can then generate a graph analogous to the force diagram shown in Fig. 2. Using specialized mathematical software (MathCad), the function g(ξ) can be defined as

$$g(\xi) := \mathrm{if}(\xi < \lambda_{z1}, \xi, \mathrm{if}(\xi < \lambda_{z1} + \lambda_a, \lambda_{z1}, \xi - \lambda_a)). \tag{41}$$

The formula for energy *E* can now be represented as follows:

$$E = 2E_1 = P_\mathrm{a}\begin{cases} \frac{\xi^2 l_c^{\,2}}{l_{z1}} \\ 2\xi l_\mathrm{c} - l_{z1} \\ 2\xi l_\mathrm{c} - l_{z1} + \frac{(\xi l_\mathrm{c} - l_{z1} - l_\mathrm{a})^2}{l_{z1}} \end{cases} \tag{42}$$

or

$$E(\xi) = P_a l_c \begin{cases} \frac{\xi^2}{\lambda_{z1}} \\ 2\xi - \lambda_{z1} \\ 2\xi - \lambda_{z1} + \frac{(\xi - \lambda_{z1} - \lambda_a)^2}{\lambda_{z1}} \end{cases}. \tag{43}$$

The resulting differential equation—Equation (39)—can be solved using the Runge-Kutta method by applying the following substitutions:

$$\dot{\xi} = y_1, \xi = y_o. \tag{44}$$

This produces a system of two first-order differential equations of the form

$$\dot{y}_o = \dot{\xi} = y_1, \dot{y}_1 = \ddot{\xi} = -wg(y_o)$$

with the following initial conditions:

$$y_o(0) = 0, y_1(0) = \frac{v}{l_c}. \tag{45}$$

The simulation results are presented in the graphs below. The following input data were assumed:
$m_1 = m = 20$ t,
$v = 36$ km/h = 10 m/s,
$\lambda = 0.7$; $E_{zd} = 62$ kJ (energy absorbed by the two Ringfeder buffers),
$l_z = 105$ mm (buffer stroke), and
$l_a = 1437$ mm (absorber stroke length).

Fig. 3 shows the distance *x(t)* traveled by the first and second vehicles from the start of the collision. The maximum value is 1.542 m and coincides with the total stroke of the absorption system l_c.

Fig. 4 shows a plot of velocity *v* as a function of displacement *x*. The vehicles are abruptly braked at the end of path *x*. The energy accumulated in the buffers and in the absorbers during the impact was plotted in order to check the correctness of the calculations. The course of variation of the function $E(\xi)$ is presented in Fig. 5.

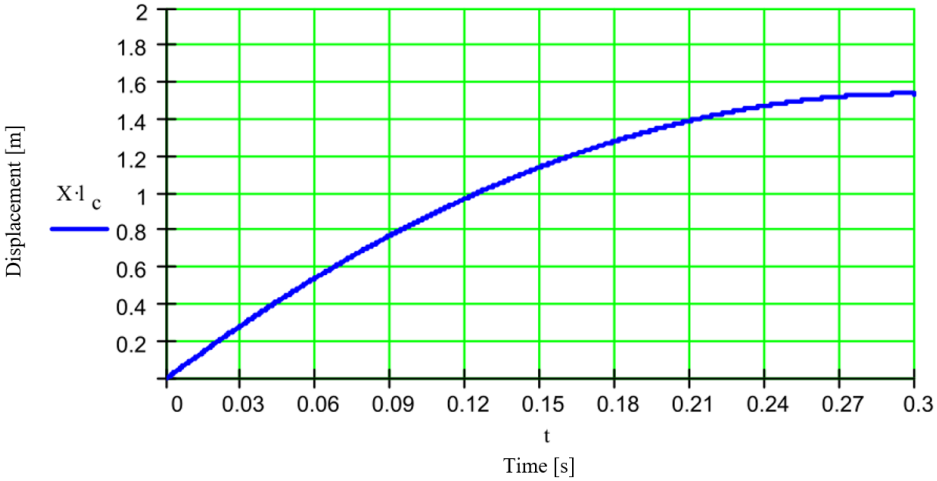

Fig. 3. Displacement x(t) [m] of the first and second vehicle from the beginning of the collision

3.3. Experimental impact with a soft absorber system

The experimental test considered here aims to calibrate the theoretical model according to Scenario 1. Instead of real masses, the test vehicles have masses m_{t1} and m_{t2}. One of the vehicles is a drag (i.e., a stationary but unbraked special test car), as shown in Fig. 1(b). It has a so-called rigid front wall without a bumper and without an absorber ($E_{t2} = 0$).

The above assumptions can be written as

$$x = x_1 - x_2, m_1 = m_{t1}, m_2 = m_{t2}, \mu_t = \frac{m_{t1}}{m_{t2}}. \quad v_1 = v, v_2 = 0 \tag{46}$$

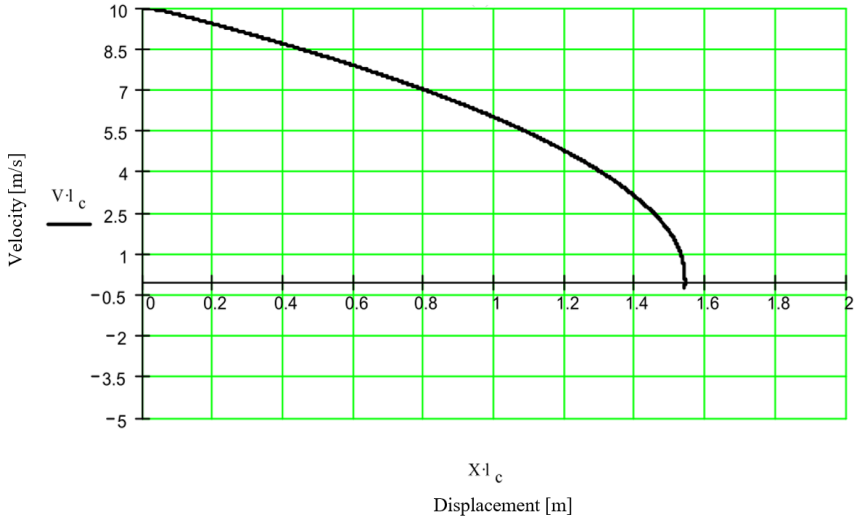

Fig. 4. Velocity V [m/s] of the first and second vehicle as a function of displacement

Fig. 5. Energy E [J] absorbed by absorption systems of both vehicles as a function of displacement

According to [15], we have two equations:

$$\begin{cases} m_{t1}v + m_{t2}0 = m_{t1}\dot{x}_1 + m_{t2}\dot{x}_2 \\ \frac{1}{2}m_{t1}v^2 = \frac{1}{2}m_{t1}\dot{x}_1^2 + \frac{1}{2}m_{t2}\dot{x}_2^2 \; E \end{cases}, \tag{47}$$

where

$$E = E_{t1} = P_a \begin{cases} \frac{1}{2}\frac{x^2}{l_{z1}} \\ x - \frac{1}{2}l_{z1} \\ x - \frac{1}{2}l_{z1} + \frac{1}{2}\frac{(x - l_{z1} - l_a)^2}{l_{z1}} \end{cases}. \tag{48}$$

From the equation of conservation of momentum, we obtain the following relationship:

$$\dot{x}_2 = \frac{m_{t1}}{m_{t2}}(v - \dot{x}_1). \tag{49}$$

Also, because

$$\dot{x} = \dot{x}_1 - \dot{x}_2, \tag{50}$$

we get

$$\dot{x} = \dot{x}_1(1 + \mu_t) - \mu_t v. \tag{51}$$

From the equation of conservation of energy and after the substitution of compound (49), the following equation is obtained:

$$m_{t1}v^2 = m_{t1}\dot{x}_1^2 + m_{t2}\left(\frac{m_{t1}}{m_{t2}}\right)^2 (v - \dot{x}_1)^2 + 2E_{t1} \tag{52}$$

or

$$v^2 = \dot{x}_1^2 + \mu_t(v^2 - 2v\dot{x}_1 + \dot{x}_1^2) + \frac{2E_{t1}}{m_{t1}}. \tag{53}$$

After differentiating both sides after the time of Equation (53), we obtain

$$0 = 2\dot{x}_1\ddot{x}_1 + \mu_t(-2v\ddot{x}_1 + 2\dot{x}_1\ddot{x}_1) + \frac{2\dot{E}_{t1}}{m_{t1}} \tag{54}$$

or

$$\ddot{x}_1[\dot{x}_1 + \mu_t(-v + \dot{x}_1)] = -\frac{\dot{E}_{t1}}{m_{t1}}. \tag{55}$$

Alternatively, if Equation (51) is used, we get

$$\ddot{x}_1\dot{x} = -\frac{\dot{E}_{t1}}{m_{t1}}. \tag{56}$$

After differentiating the right-hand side of Equation (48), we obtain the formula for the time derivative of the function Et_1:

$$\dot{E}_{t1} = \frac{P_a}{2l_{z1}}\begin{cases} 2x\,\dot{x} \\ 2\dot{x}\,l_{z1} \\ 2\dot{x}\,l_{z1} + 2(x - l_{z1} - l_a)\dot{x} \end{cases}. \tag{57}$$

Alternatively, after transformations, we get the formula

$$\dot{E}_1 = \frac{P_a\dot{x}}{l_{z1}}\begin{cases} x \\ l_{z1} \\ x - l_a \end{cases}. \tag{58}$$

Thus, the differential equation—Equation (56)—takes the form

$$\ddot{x}_1\dot{x} = -w\dot{x}\begin{cases} x \\ l_{z1} \\ x - l_a \end{cases}, \tag{59}$$

where the following substitution has been made:

$$\frac{P_a}{m_{t1}l_{z1}} = w \tag{60}$$

After differentiating Equation (51) on both sides, we obtain

$$\ddot{x} = \ddot{x}_1(1 + \mu_t). \tag{61}$$

Thus, ultimately,

$$\ddot{x} = -w(1 + \mu_t)\begin{cases} x \\ l_{z1} \\ x - l_a \end{cases}. \tag{62}$$

The resulting differential equation can be solved using the Runge-Kutta method by applying the following substitutions:

$$\frac{x}{l_c} = y_o, \frac{\dot{x}}{l_c} = y_1. \tag{63}$$

This produces a system of two first-order differential equations of the following form:

$$\dot{y}_o = y_1, \dot{y}_1 = -w(1+\mu_t)g(y_o), \tag{64}$$

where

$$g(\xi) = \begin{cases} \xi & \text{dla } 0 \le \xi \le \lambda_{z1} \\ \lambda_{z1} & \text{dla } \lambda_{z1} < \xi \le \lambda_{z1} + \lambda_a \\ \xi - \lambda_a & \text{dla } \lambda_{z1} + \lambda_a < \xi \le \lambda_c \end{cases}. \tag{65}$$

Equation (48) for the energy E absorbed by the absorption system can now be represented as follows:

$$E(\xi) = \frac{P_a l_c}{2} \begin{cases} \frac{\xi^2}{\lambda_{z1}} \\ 2\xi - \lambda_{z1} \\ 2\xi - \lambda_{z1} + \frac{(\xi - \lambda_{z1} - \lambda_a)^2}{\lambda_{z1}} \end{cases}. \tag{66}$$

The system of equations must have the following initial conditions:

$$y_o(0) = 0, y_1(0) = \omega, \tag{67}$$

where the following was substituted:

$$\frac{v}{l_c} = \omega. \tag{68}$$

The sought unknowns can be determined according to Equations (49) and (50):

$$\dot{x}_1 = \frac{\dot{x} + \mu_t v}{1+\mu_t} \tag{69}$$

and

$$\dot{x}_2 = \dot{x}_1 - \dot{x} = \frac{\mu_t(v - \dot{x})}{1+\mu_t}. \tag{70}$$

By integrating both sides of the above equations, we get the displacement formulae:

$$x_1 = \frac{x + \mu_t v t}{1+\mu_t} + C_1, x_2 = x_1 - x + C_2, \tag{71}$$

where the integration constants (with respect to (67)) take the values $C_1 = C_2 = 0$.

The simulation results are presented in the graphs below. The following input data were assumed:

m_{t1} = 30 t (weight of the oncoming vehicle),
m_{t2} = 25 t (weight of the blocking vehicle),
$v_1 = v$ = 36 km/h = 10 m/s,
λ = 0,7; (auxiliary quantity),
E_{zd} = 62 kJ (energy absorbed by 2 Ringfeder buffers),
l_z = 105 mm (buffer stroke), and
l_a = 1437 mm (absorber stroke length).

Fig. 6 shows the distance as a function of time $x(\tau)$ traveled by the first vehicle relative to the second vehicle since the beginning of the collision (τ = time in s).

Fig. 7. shows the course of the speed of the run-up vehicle v_1 and the run-up vehicle v_2, both as a function of time and displacement x. The kinetic energy of both vehicles $E_{t1}(x)$, $E_{t2}(x)$ and the energy absorbed by the absorption system E(x) are shown in Fig. 8.

The obtained mathematical apparatus can be enriched with more accurate data on the absorption system and other data (e.g., further data on the parameters of the tested vehicle). Described simulation analysis tool based on mathematical formulas is helpful in studying the influence of various factors on the course of crashes and thus can be used to determine the optimum values of speed and ballast masses of test vehicles [17-19].

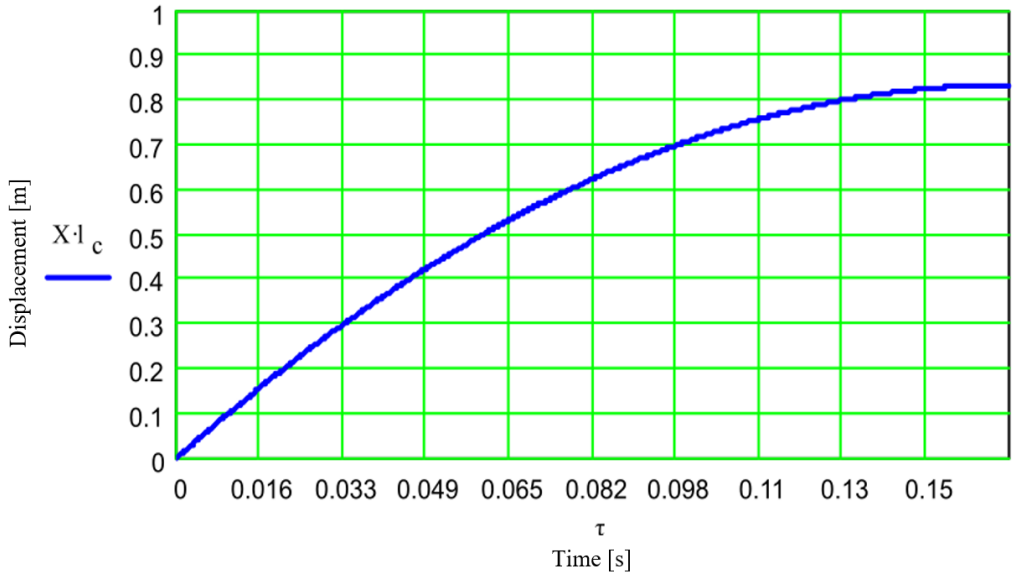

Fig. 6. Displacement x [m] covered by the first vehicle in relation to the second, time [s]

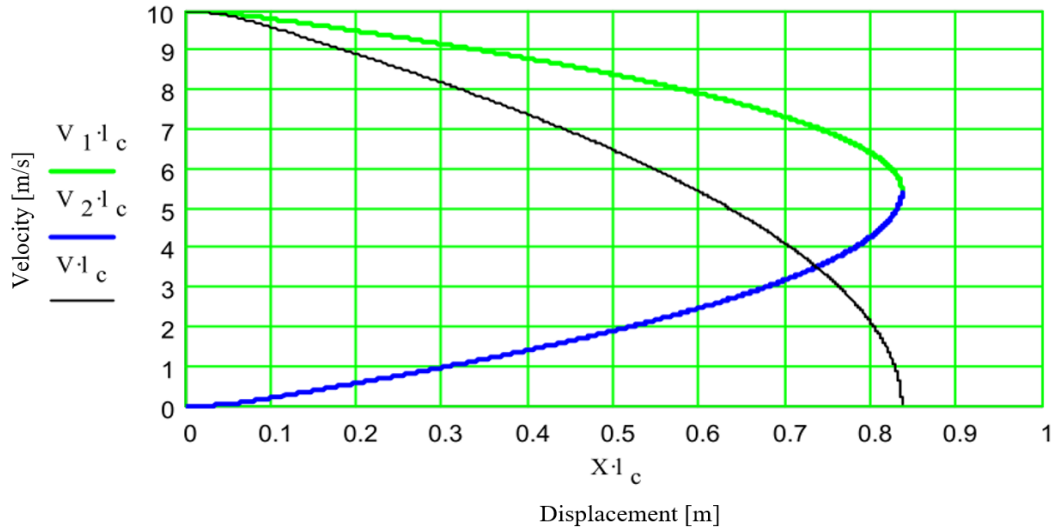

Fig. 7. Velocities of both vehicles $v_1(x), v_2(x)$ [m/s] and relative speed $v(x)$ [m/s], x – displacement [m]

4. CONCLUSIONS

The method of simulating crash tests of rail vehicles presented in the paper makes it possible to check the behavior of the absorption system of a railway vehicle during a collision. Calculations carried out on the example of an absorption system consisting of Ringfeder-type bumpers and a soft absorber (honeycomb) make it possible to draw the following conclusions:

- The developed mathematical model based on the requirements of EN 15227:2020 Railway applications - Crashworthiness requirements for rail vehicles allows for the determination of basic crash parameters such as the distance traveled by vehicles since the impact, their speeds, and the energy absorbed by the absorbing elements.
- The possibility of including the characteristics of different types of absorbers (i.e., crash bumper, two- and three-stage absorber) in the model allows rolling stock manufacturers to verify the impact strength of the vehicle.

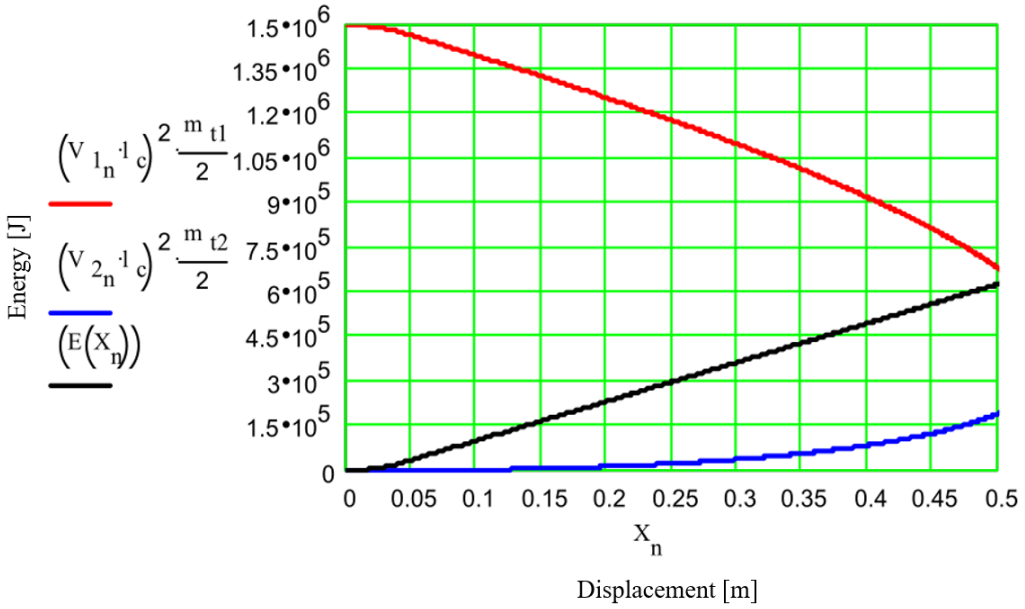

Fig. 8. Kinetic energy of both vehicles $E_{t1}(x), E_{t2}(x)$ [J] and energy absorbed by the absorption system $E(x)$ [J] x – displacement [m]

– The mathematical model developed may be used as a preliminary method for testing the behavior of railway vehicles in a collision with another railway vehicle or with obstacles in accordance with the scenarios contained in EN 15227:2020. Currently, the most commonly used method of simulating crash tests is analysis using the finite element method. However, its use at the vehicle design stage is very difficult, as it requires the verification of different versions of the vehicle prototype with different absorbers. The developed method allows for a significant reduction in the time and cost of tests, and the finite element method analysis may constitute the final stage of verification of calculations.

In conclusion, implementing the method described in this paper can significantly contribute to optimizing the time and costs to be devoted to the substantive preparation of real crash tests of rail vehicles in accordance with the requirements of EN 15227:2020. The model described in the present work can be used for various types of rail vehicles.

References

1. *Railway safety statistics in the EU.* Available at: https://ec.europa.eu/eurostat/statistics-explained/index.php?
2. Amraei, M. & Shahravi, M. & Noori, Z. & Lenjani, A. Application of aluminium honeycomb sandwich panel as an energy absorber of high-speed train nose. *Journal of Composite Materials.* 2013. Vol. 48. No. 9. P. 1027–1037.
3. PN-EN 15227:2020. *Kolejnictwo - Wymagania zderzeniowe dla pojazdów szynowych*. Warszawa: Polski Komitet Normalizacyjny. [In Polish: *Railway applications - Crashworthiness requirements for rail vehicles*. Warsaw: Polish Committee of Standardization].
4. Simic, G. & Lucanin, V. & Milkovic, D. Elements of passive safety of railway vehicles in collision. *International Journal of Crashworthiness.* 2006. Vol. 11. No. 4. P. 357-369.
5. Li, B. & Lu, Z. & Yan, K. & Lu, S. & Kong, L. & Xu, P. Experimental study of honeycomb energy-absorbing device for high-speed trains. *Proceedings of the Institution Mechanical Engineers, Part F: Journal of Rapid Transit.* 2019. Vol. 234. No. 10. P. 1170–1183.

6. Hong, S. & Pan, J. & Tyan, T. & Prasad, P. Dynamic crush behaviors of aluminum honeycomb specimens under compression dominant inclined loads. *International Journal of Plasticity.* 2008. Vol. 24(1). P. 89-117.
7. Xie, S. & Liang, X. & Zhou, H. Design and analysis of a composite energy-absorbing structure for use on railway vehicles. *Proceedings of the Institution Mechanical Engineers. Part F: Journal of Rapid Transit.* 2015. Vol. 230. No. 3. P. 825–839.
8. Amraei, M. & Shahravi, M. Aluminium honeycomb energy absorber for high-speed train nose. In: *Proceedings of the ASME 11th Biennial Conference on Engineering Systems Design and Analysis.* 2012. Vol. 3. P. 93-99.
9. Xie, S. & Li, H. & Yang, W. & Wang, N. Crashworthiness optimization of a composite energy-absorbing structure for railway vehicles. *Structural and Multidisciplinary Optimization.* 2018. Vol. 57. P. 1793-1807.
10. Tang, Z. & Liu, S. & Zhang, Z. Energy absorption properties of non-convex multi-corner thin-walled columns. *Thin-Walled Structures*. 2012. Vol. 51. P. 112-120.
11. Nagel, G.M. & Thambiratnam, D.P. Computer simulation and energy absorption of tapered thin-walled rectangular tubes. *Thin-Walled Structures*. 200. Vol. 43(8). P. 1225-1242.
12. Alexander, J.M. An approximate analysis of the collapse of thin cylindrical shells under axial loading. *Mechanics & Applied Mathematics*. 1960. Vol. 13(1). P. 10-15.
13. Ambrosio, J. Crash analysis and dynamical behaviour of light road and rail vehicles. *Vehicle System Dynamics*. 2005. Vol. 6(7). P. 385-411.
14. Deepak, S. & Vasanthanathan, A. & Nagaraj, P. Finite Element Modelling and Simulation of Train Car Body Structure Using LS-Dyna. *Applied Mechanics and Materials*. 2015. Vol. 787. P. 270-274.
15. Gryboś, R. *Teoria uderzenia w dyskretnych układach mechanicznych.* [In Polish: *Impact theory in discrete mechanical systems*]. PWN Warszawa. 1969. Instytut Podstawowych Problemów Techniki Polskiej Akademii Nauk. Biblioteka mechaniki stosowanej.
16. PN-EN 12663-1+A1:2015-01. *Kolejnictwo - Wymagania konstrukcyjno-wytrzymałościowe dotyczące pudeł kolejowych pojazdów szynowych - Część 1: Lokomotywy i tabor pasażerski (i metoda alternatywna dla wagonów towarowych).* Warszawa: Polski Komitet Normalizacyjny. [In Polish: *Railway applications - Structural requirements of railway vehicle bodies - Part 1: Locomotives and passenger rolling stock (and alternative method for freight wagons)*. Warsaw: Polish Committee of Standardization].
17. Groll, W. & Sanecki, H. Crash tests - theory and practice. IN: *UN-ESCAP Ministerial Conference on Transport*. Busan (S. Korea). November 8-9th 2006.
18. Sanecki, H. Experience in full scale tests of passive safety assessment of rolling stock. In: *SAMNET. Workshop on Railway Safety Management Systems.* Warsaw. June 30th 2005.
19. Dias, J.P. & Pereira, M.S. Optimization methods for crashworthiness design using multibody models. *Comput Struct*. 2004. Vol. 82. P. 1371–1380.

Received 03.01.2022; accepted in revised form 31.08.2023